Nano Res. 2010, 3(12): 863–873
DOI 10.1007/s12274-010-0057-x
Research Article

ISSN 1998-0124
CN 11-5974/O4

Ag_2Se Complex Nanostructures with Photocatalytic Activity and Superhydrophobicity

Huaqiang Cao[1] (✉), Yujiang Xiao[1,2], Yuexiang Lu[1], Jiefu Yin[1], Baojun Li[1], Shuisheng Wu[1,3], and Xiaoming Wu[1,4]

[1] Department of Chemistry, Tsinghua University, Beijing 100084, China
[2] School of Chemistry and Chemical Engineering, Central South University, Changsha 410083, China
[3] College of Chemistry and Chemical Engineering, Hunan University, Changsha 410082, China
[4] School of Chemistry and Chemical Engineering, Nanjing University, Nanjing 210093, China

Received: 2 July 2010 / Revised: 11 September 2010 / Accepted: 9 October 2010

ABSTRACT

Single-crystalline Ag_2Se complex nanostructures have been synthesized via a solvothermal route in which selenophene (C_4H_4Se) as a selenylation source reacts with $AgNO_3$ at a temperature of 240 °C. An orthorhombic phase β-Ag_2Se nanostructure was identified by X-ray diffraction (XRD), Raman spectroscopy, field emission scanning electron microscopy (FE-SEM), high resolution transmission electron microscopy (HRTEM), and photoluminescence (PL) spectroscopy. The wettability of the as-synthesized β-Ag_2Se nanostructure was studied by measurement of the water contact angle (CA). Static water CA values of over 150° were obtained, which can be attributed to the β-Ag_2Se complex nanostructure having a combination of micro- and nanostructures. The superhydrophobic Ag_2Se nanostructure may find applications in self-cleaning. Additionally, the photocatalytic activity of the as-synthesized β-Ag_2Se nanostructure was evaluated by photodegradation of rhodamine B (RhB) dye under ultraviolet (UV) light irradiation.

KEYWORDS

Nanostructures, photocatalytic, photoluminescence, superhydrophobicity, silver selenide

1. Introduction

Creation of complex nanostructures on multiple-length scales with novel properties and functionalities will be one of the most important scientific and technical challenges in the coming years [1–3]. Many inorganic complex nanostructures with novel properties and applications have been synthesized through self-assembly routes. In particular, the superhydrophobicity of nanostructures on which water forms a nearly perfect spherical bead and rolls off—known as the lotus effect [4]—has aroused great interest. The lotus effect can be attributed to hierarchical micro- and nanostructures on the surface of a material. This has inspired the construction of complex inorganic nanostructures having superhydrophobicity. Herein,we report for the first time the self-assembly of semiconductor Ag_2Se nanoparticles into a plate-like nanostructure.

Ag_2Se, an important band-gap semiconductor, can exist in two polymorphs at atmospheric pressure: a low-temperature orthorhmobic phase (β-Ag_2Se) with a narrow band-gap of 70 meV at 0 K, and a high-temperature cubic phase α-Ag_2Se, with a transition

Address correspondence to hqcao@mail.tsinghua.edu.cn

temperature of 135 °C [5]. β-Ag_2Se is used as a photosensitizer in photographic films and in thermochromic materials due to its relatively high Seebeck coefficient, low lattice thermal conductivity, and high electrical conductivity [6], while α-Ag_2Se, being a superionic conductor, finds application in solid electrolytes in photochargable secondary batteries [7]. Various shapes of Ag_2Se nano- and microstructures have been obtained by different methods, such as a solution-phase synthesis approach [5], a sacrificial template route [8], a template-engaged reaction method [9], and a hydrothermal route [10]. The study of possible industrial applications of such nanomaterials has also received tremendous attention. Here we demonstrate for the first time, to the best of our knowledge, that an as-synthesized Ag_2Se plate-like nanostructure possesses both superhydrophobicity and photocatalytic activity.

The contact angle (CA) is the angle formed by a liquid drop at the three-phase boundary where a liquid, gas and solid intersect. The measurement of CA is very important in the paint and coating industries [11]. When the CA is less than 90°, the liquid is said to wet the solid, while a surface with a CA greater than 90° is said to be non-wetting, and materials with CA values larger than 150° are said to be superhydrophobic [4]. In fact, the interactions between solids and liquids play a key role in understanding the chemical and physical processes in many industries—for example, a car body coating can be evaluated by measuring the hydrophobicity of the lacquer surface. Recently, CA measurements have been used to evaluate the cleanliness of semiconductor surfaces in the electronics industry, which is of great potential interest for the rapidly developing nanotechnology field [4]. In recent years, the focus of nanotechnology research has been steadily moving away from the preparation of high-quality nanomaterials and the understanding of their physicochemical properties, to the field of applications [12], especially, to industrial applications [13–16]. Compared with superhydrophobic surfaces composed of organic polymer coatings, such as poly(methyl methacrylate) (PMMA) fibers [17], rambutan-like hollow spheres of polyaniline [18], and poly(*N*-isopropylacrylamide)-*co*-poly(acrylamido-phenylboronic acid) copolymer films [19], superhydrophobic inorganic nanostructures, such as Ag_2Se, can withstand higher temperatures and have good tolerance to acids and alkalis, which suggests they may have a wider range of applications.

2. Results and discussion

The phase structure and purity of the as-synthesized materials (see Experimental section below) were studied by X-ray diffraction (XRD) and Raman spectroscopy. Figure 1(a) shows a representative XRD pattern of the as-synthesized sample **S-1** (see Table 1 for details of the synthesis conditions for the different samples). XRD demonstrates that the sample is single-phase orthorhombic β-Ag_2Se with lattice constants of a = 4.333 Å, b = 7.062 Å, and c = 7.764 Å (JCPDS file No. 24-1041). The Raman spectrum (Fig. 1(b)) of the as-synthesized sample **S-1** shows a peak at 132 cm^{-1} which is characteristic of Ag–Se bond formation [20–22]. A series of products using different concentrations and molar ratios of Ag^+ to C_4H_4Se, and reaction temperatures and times were prepared (Table 1 & Fig. S-1 in the Electronic Supplementary Material (ESM)).

The morphology and structure were further studied by field emission scanning electron microscopy (FE-SEM) and high-resolution transmission electron microscopy (HRTEM). Typical FE-SEM images (Figs. 2(a) and 2(b)) show that the as-synthesized Ag_2Se particles in sample **S-1** cluster into plate-like aggregates ca. 33 nm in thickness and ca. 900 nm in size. ZnO with a similar bowl-like nanostructure has been reported by Krishna and co-workers [3]. HRTEM images (Figs. 2(c) and 2(d)) show a clearly visible set of lattice fringes with a period ~0.24 nm, characteristic of the {013} planes of β-Ag_2Se. The selected-area electron diffraction (SAED) pattern (top-right inset in Fig. 2(c)) further confirms that the material has a single crystalline structure.

A possible mechanism for the growth of the Ag_2Se nanostructures is as follows. It is usually believed that the growth of nanostructures in solution involves two important processes, namely nucleation followed by growth [23]. In the case of our Ag_2Se samples, these two processes are followed by assembly of the plate-shaped structure. In the first stage, Ag_2Se nuclei are

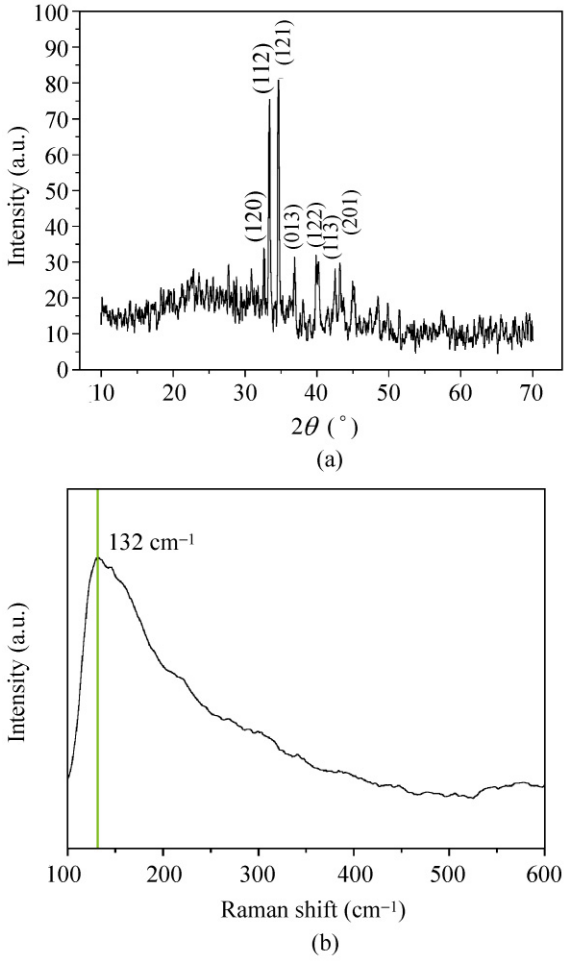

Figure 1 (a) XRD pattern and (b) Raman spectrum of the as-synthesized sample **S-1**

Table 1 Experimental parameters for the synthesis of the different products

Sample No.	Ag+/C_4H_4Se (molar ratio)	Reaction temperature (°C)	Reaction time (h)
S-1	4: 0.5	240	10
S-2	1: 0.5	240	10
S-3	1: 1	240	10
S-4	2: 1	240	10
S-5	1: 0.5	240	5
S-6	1: 0.5	240	24
S-7	0.5: 0.25	240	10

formed in solution through heat treatment of the mixture containing Ag^+ and C_4H_4Se. The freshly Ag_2Se nuclei are thermodynamically unstable due to their high surface energy and tend to aggregate, driven by the minimization of interfacial energy [24],

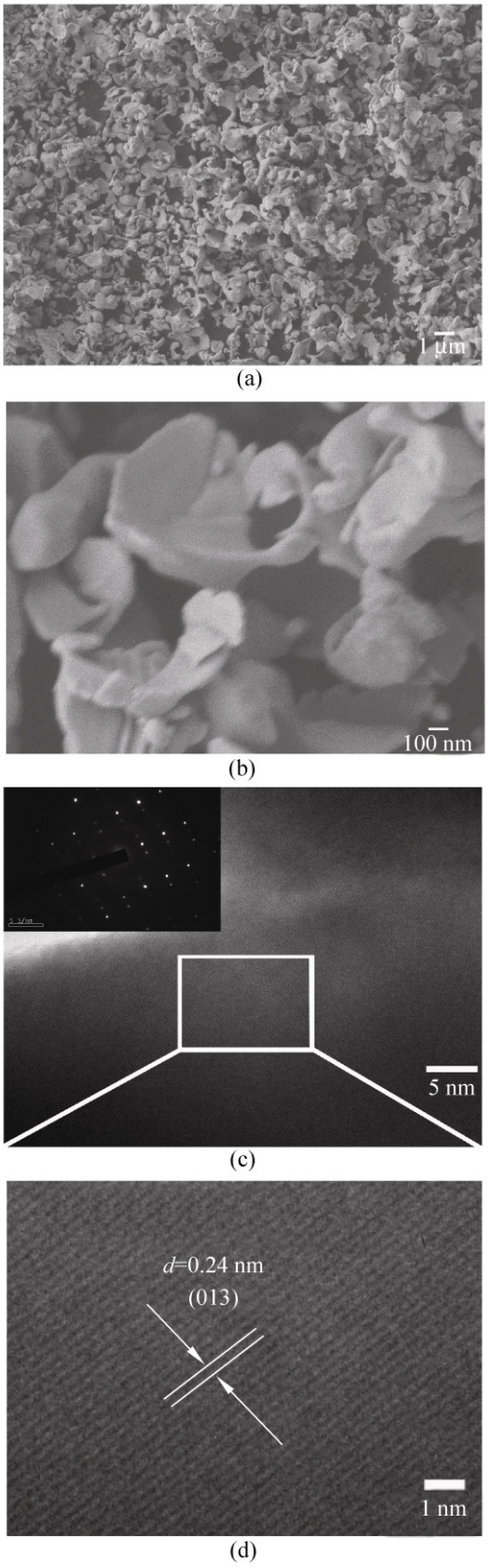

Figure 2 (a) and (b) FE-SEM images and (c) and (d) HRTEM images of as-synthesized As_2Se sample **S-1**. The inset in (c) shows the corresponding SAED pattern

which leads to larger particles. Assembly of these larger particles occurs in the third stage. All self-assembling systems are driven by energy minimization [25]. In this case, the van der Waals interaction between Ag_2Se particles can be regarded as the driving force of the self-assembly process.

We found that the Ag^+/C_4H_4Se molar ratio significantly affects the morphology of the products. FE-SEM and SEM images of Ag_2Se prepared with an Ag^+/C_4H_4Se molar ratio of 4:0.5 (**S-1**) are displayed in Figs. 1, 2, and S-1(a) in the ESM. The majority of Ag_2Se particles have sizes in the range 200–300 nm. The FE-SEM and SEM images show that the plate-shaped particles tended to aggregate. We varied the Ag^+/C_4H_4Se molar ratio in the synthesis mixture with the other conditions remaining constant. When the Ag^+/C_4H_4Se molar ratio was 1:0.5 (**S-2**, Fig. S-1(b) in the ESM), the predominant size of the particles was ~300 nm. This suggests that a high Ag^+/C_4H_4Se molar ratio favors the aggregation of Ag_2Se particles to afford complex nanostructures. The predominant size of Ag_2Se with an Ag^+/C_4H_4Se molar ratio of 1:1 (**S-3**, Figs. S-1(c) and S-1(h) in the ESM) was in the range 300-400 nm. Increasing the Ag^+/C_4H_4Se molar ratio to 2:1 (**S-4**, Fig. S-1(d) in the ESM), gave particles with similar size to that of sample **S-3**.

Increasing the reaction time from 5 h (**S-5**, Fig. S-1(e) in the ESM) to 10 h (**S-2**, Fig. S-1(b) in the ESM) or 24 h (**S-6**, Fig. S-1(f) in the ESM) without changing the other conditions, gave particles with predominant sizes in the range 200–300 nm, 300 nm, and 500 nm, respectively. Particle aggregation was observed in **S-6**. This suggests that prolonged reaction times favor both particle growth and aggregation.

We also investigated the effect of varying the reactant concentration when the molar ratio of Ag^+/C_4H_4Se was kept fixed. Increasing the reactant concentration (from **S-7** (Fig. S-1(g) in the ESM) to **S-5** (Fig. S-1(e) in the ESM) to **S-4** (Fig. S-1(d) in the ESM)) favored the formation of larger particles.

The optical properties of as-synthesized Ag_2Se were investigated by ultraviolet–visiable (UV–vis) and photoluminescence (PL) spectroscopy. The UV–vis absorption properties of the the Ag_2Se sample were investigated by dissolving Ag_2Se in ethanol (0.5 mg/mL) (Fig. 3(a)). The UV–vis spectrum showed a broad absorption peak centered at a wavelength of about 755 nm (corresponding to a photon energy of 1.64 eV). This value is similar to that reported for Ag_2Se nanotubes [26].

The room temperature PL spectra of as-synthesized Ag_2Se nanobowls with different excitation wavelengths (λ_{ex} = 275, 280, 285, 290, and 295 nm) are shown in Fig. 3(b). All the PL spectra exhibit three emission peaks: a violet emission centered at ca. 418 nm (2.96 eV), a blue emission centered at ca. 460 nm (2.69 eV), and an indigo blue emission centered at ca. 495 nm (2.50 eV). The emission peaks are almost independent of the excitation wavelength, with the maximum PL intensity observed for λ_{ex} = 275 nm. These results indicate that the PL emission comes from the as-synthesized complex Ag_2Se nanostructures and not from impurities [27]. Similar results have been observed by Zhang and co-workers for Ag_2Se nanotubes [26].

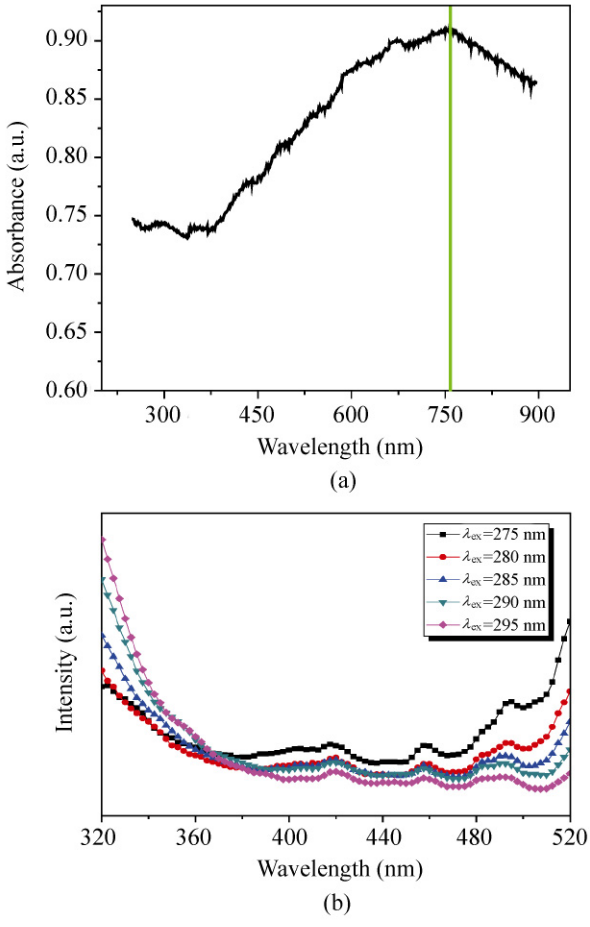

Figure 3 (a) UV–vis spectrum and (b) PL spectra with different excitation wavelengths of as-synthesized Ag_2Se nanostructures

Dyes in the effluents from the textile and paper industries are regarded as major environmental pollutants, because of their non-biodegradability and toxicity. Rhodamine B (RhB) is one of the most important cationic xanthene dyes and is widely used in the printing, textile, and photographic industries [28]. Semiconductor photocatalysts have been extensively studied as catalysts for the degradation of environmental pollutants [29]. It is known that RhB is very stable and is usually not biodegradable in waste water. The photocatalytic activities of the as-synthesized Ag_2Se nanostructure were evaluated for the degradation of RhB dye solution (10^{-5} mol/L) with UV light irradiation at different pH. The intensity of the characteristic absorption peak of RhB at λ = 553 nm was selected to monitor the photocatalytic degradation process. As control experiments, we carried out the degradation of RhB in aqueous solution at pH 7 in the presence of Ag_2Se nanoplates in darkness (Fig. S-2(a) in the ESM) and in the absence of Ag_2Se nanoplates at pH 7 under UV light irradiation (Fig. S-2(b) in the ESM). These experiments showed that the degradation of RhB over a period of 15 h was relatively low, being <12% in each case.

However, RhB underwent an obvious photodegradation in the presence of Ag_2Se nanoplates under UV irradiation. Figure 4(a) shows the UV–vis spectral changes during the photodegradation of RhB in the presence of Ag_2Se nanoplates at pH 7. After 15 h, the degradation of RhB reached 89.8%. The

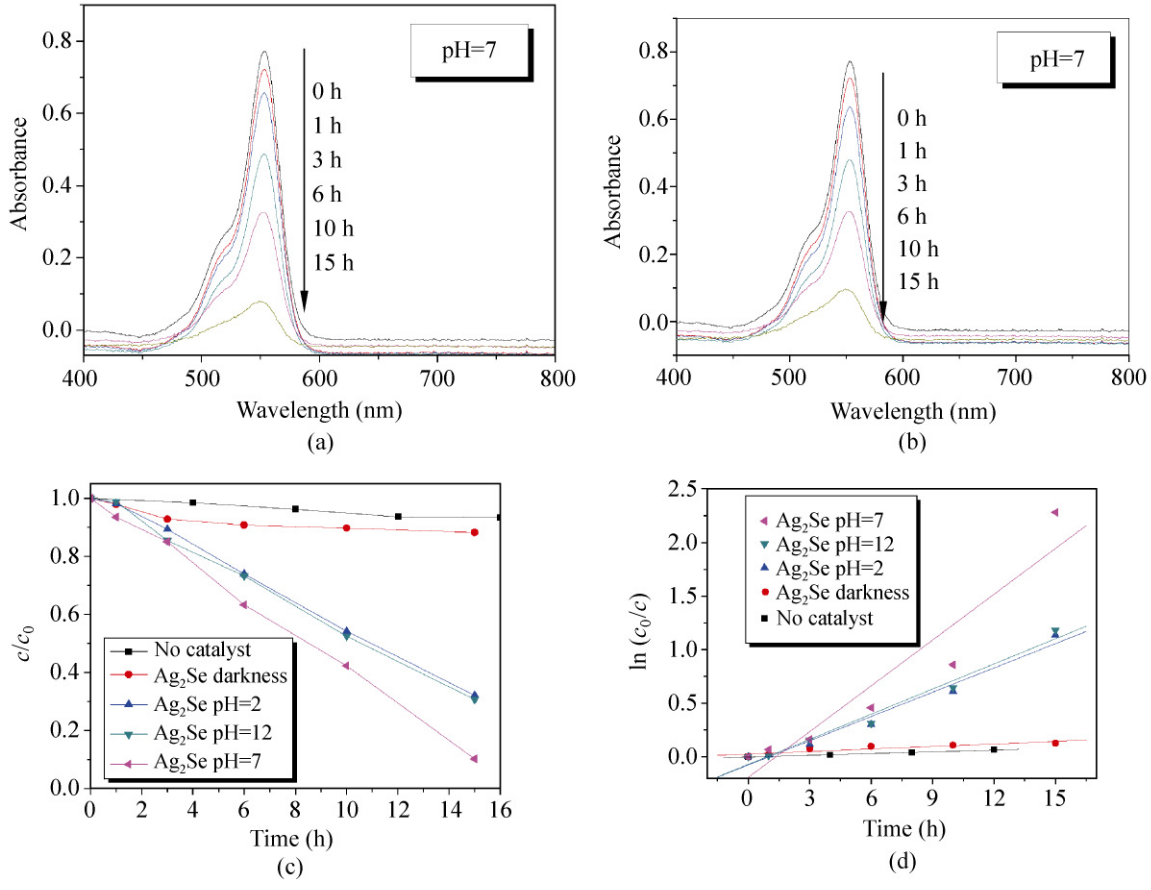

Figure 4 Temporal UV–vis absorption spectral changes observed for RhB solutions at pH 7: (a) in the presence of Ag_2Se nanoplates (**S-1**); (b) in the presence of reused Ag_2Se nanoplates (**S-1**) after washing and drying; (c) photodegradation curves of RhB in water in the presence of Ag_2Se nanoplates at different pH values under UV irradiation, without adding any Ag_2Se catalyst under UV irradiation, and in the presence of Ag_2Se nanoplates in darkness; (d) selected fitting results using the pseudo-first-order reaction equation. The initial RhB concentration was 10^{-5} mol/L in each case

XRD pattern (Fig. S-3 in the ESM) of the catalyst after the reaction was identical to that of the pristine β-Ag_2Se catalyst, showing that the material is stable under photocatalytic conditions. This was confirmed by washing the used β-Ag_2Se catalyst three times with deionized water and absolute alcohol followed by drying at 80 °C for 4 h, and then repeating the photodegradation reaction under the same conditions as above. The degradation of RhB (Fig. 4(b)) reached 87.5% after 15 h, similar to the value for the fresh catalyst.

For a pseudo-first-order reaction, the concentration changes can be fitted by the equation

$$\ln c_0/c = kt \quad (1)$$

where c_0 and c indicate the initial RhB concentration and that after irradiation time t, respectively, and k is the reaction rate constant [30]. Figure 4(d) shows that there is a linear relationship between $\ln c_0/c$ and t, confirming that the photodegradation reaction is indeed pseudo-first-order. Under UV light irradiation, the pseudo-first-order rate constants for the photodegradation of RhB are 0.0756 h^{-1} (i.e., 1.260×10^{-3} min^{-1}), 0.0783 h^{-1} (i.e., 1.305×10^{-3} min^{-1}), and 0.1427 h^{-1} (i.e., 2.378×10^{-3} min^{-1}) at pH values of 2, 12, and 7, respectively (Fig. 4(c)). The pseudo-first-order rate constants for the degradation of RhB without catalyst or in darkness, however, are only 0.0055 h^{-1} (i.e., 9.167×10^{-5} min^{-1}) and 0.0078 h^{-1} (i.e., 1.300×10^{-4} min^{-1}), respectively. To the best of our knowledge, this is the first time it has been demonstrated that semiconductor Ag_2Se is an active catalyst for the photodegradation of RhB.

The blank experiments showed that the degradation of RhB was negligible in darkness or in the absence of Ag_2Se nanoplates. The pH value of the RhB solution also had a significant influence on the photocatalytic activity. After 15 h irradiation at pH 2 or 12, the degradation of RhB reached 69.3% and 67.9%, respectively (Figs. S-2(c) and S-2(d) in the ESM), whereas at pH 7 the degradation of RhB reached 89.8%. These results suggest that neutral conditions favor the degradation of RhB. The degradation of RhB reached only 11.6% after adding the as-synthesized Ag_2Se nanostructure under visible light irradiation at pH 7 (Fig. S-2(e) in the ESM).

In a further control experiment, we also evaluated the photodegradation of RhB in the presence of spherical Ag_2Se particles (**S-3**, Figs. S-2(c) and S-2(f) in the ESM). After 15 h, the degradation of RhB only reached 60.3%. This shows that the particle shape has a great effect on the degradation, with the presence of a larger number of active sites on the surface of Ag_2Se nanoplates being responsible for their higher activity.

It is known that β-Ag_2Se is an n-type semiconductor [31, 32]. After activating the Ag_2Se nanoplates by UV irradiation with photon energies which match, or exceed, the band-gap energy (a wavelength which matches, or is shorter than, the absorption edge for β-Ag_2Se), conduction-band electrons (e^-) and valence-band holes (h^+) pairs are generated at the surface of Ag_2Se nanostructures, as shown in Eq. (2). An electron (e^-) is excited from the valence band into the conduction band, generating a hole (h^+) when a photon with an energy of $h\nu$ matches or exceeds the band-gap energy, E_g, of the semiconductor Ag_2Se.

$$2Ag_2Se + h\nu \longrightarrow Ag_2Se(e^-) + Ag_2Se(h^+) \quad (2)$$

Holes can react with water adsorbed on the surface of semiconductor Ag_2Se to generate highly reactive hydroxyl radicals (·OH), while O_2 acts as an electron acceptor to generate a superoxide anion radical ($\cdot O_2^-$). Also the $\cdot O_2^-$ may act as oxidizing agent or as an additional source of ·OH, as shown in Eqs. (3)–(5) [33, 34]:

$$H_2O + Ag_2Se(h^+) \longrightarrow \cdot OH + H^+ + Ag_2Se \quad (3)$$

$$O_2 + Ag_2Se(e^-) \longrightarrow \cdot O_2^- + Ag_2Se \quad (4)$$

$$\cdot O_2^- + H^+ \longrightarrow \cdot OOH \quad (5)$$

These radicals have extremely strong oxidizing ability and are able to degrade the RhB dye [35]:

$$RhB + O_2/\cdot O_2^-/\cdot OH/\cdot OOH \longrightarrow (\text{intermediates}) \longrightarrow \text{degradation products} \quad (6)$$

It has been demonstrated that a large surface area helps to increase the number of photocatalytic reaction sites and promote the efficiency of the electron–hole separation [36].

The experimental data show that neutral conditions favor the degradation of RhB, while both acid and alkaline conditions are less favourable for degradation of RhB. A similar phenomenon has been observed by other groups for other semiconductors [37–39]. The photocatalytic behaviour of semiconductors is mainly dependent upon the separation of photogenerated electron–hole pairs and transfer of the separated electrons from the photocatalyst to the organic dye through defects on the surface of photocatalyst [39, 40]. This suggests that both acid and alkaline conditions can inhibit the formation of defects on the surface of Ag_2Se nanostructures.

The wettability of glass modified by the as-synthesized Ag_2Se nanoplates was determined by CA measurements. In the first step, a glass surface modified by Ag_2Se nanoplates was fabricated by slow evaporation of a dilute ethanol dispersion of nanostructured Ag_2Se on glass, followed by drying at 30 ℃ for 15 min. The coating process was carried out either 5 or 9 times. As shown in Figs. 5(a) and 5(b), the CA values were 146.7°(148° ± 1.3°, Fig. 5(a)) and 145.4° (140.7° ± 4.7°, Fig. 5(b)) for 5 and 9 coating cycles, respectively. If the glass modified by the as-synthesized Ag_2Se nanoplates was further treated with an ethanol solution of *n*-dodecanethiol [*v*(*n*-dodecanethiol): *v*(ethanol) = 1: 3] for 1 h at room temperature, followed by drying at 80 ℃ for 3 h, the CA values increased to over 150°. As shown in Figs. 5(c)–5(f), the CA values were 126.8° (unstable, Fig. 5(c)), 148.7° (148.5° ± 0.8°, Fig. 5(d)), 151.7(152.4° ± 0.7°, Fig. 5(e)), 151.0° (151.5° ± 0.5°, Fig. 5(f)), 151.4° (151.8° ± 0.4°, Fig. 5(g)), and 151.6° (151.8° ± 0.2°, Fig. 5(h)), for 1, 3, 5, 7, 9, and 11 coating cycles, respectively. The CA values were also larger than 150° after the glass modified by as-synthesized Ag_2Se nanoplates was subsequently treated with a methanol solution of 2% (*v*/*v*) 1H,1H,2H,2H-perfluorodecyltriethoxysilane [$(C_2H_5O)_3Si(CH_2)_2C_8F_{17}$] for 1 h at room temperature, followed by drying at 120 ℃ for 1 h. As shown in Figs. 5(i)–5(m), the CA values were 145.2° (145.1° ± 1.0°, Fig. 5(i)), 152.1° (152.4° ± 1.1°, Fig. 5(j)), 151.2° (151.5° ± 0.3°, Fig. 5(k)), 151.3° (150.8° ± 0.6°, Fig. 5(l)), and 152.8° (152.8° ± 0°, Fig. 5(m)) for 1, 3, 5, 7, and 9 coating cycles, respectively [41–51]. The results indicate that the number of coating cycles can affect the CA values. This is because surface modification using as-synthesized Ag_2Se nanoplates can influence the roughness of the surface of the glass, which leads to the observed changes in wettability.

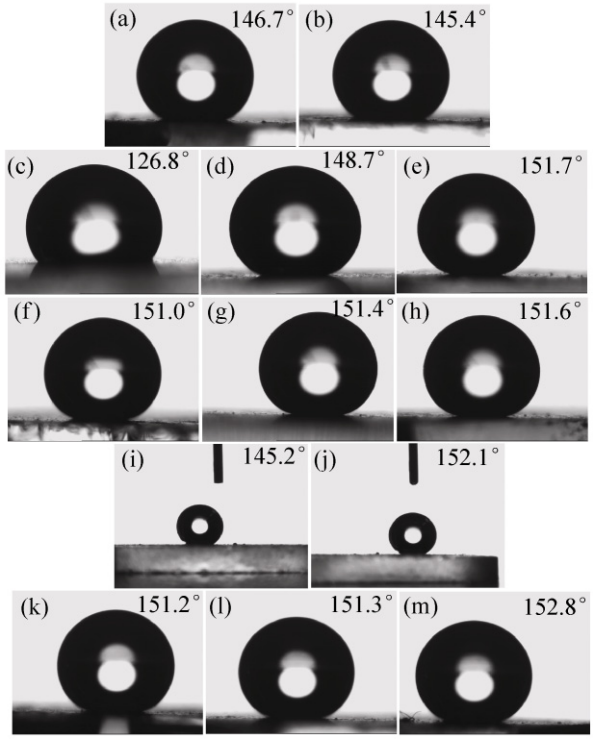

Figure 5 Surface wetting behaviour of glass modified by the as-synthesized Ag_2Se nanostructures. Water CA measurements of glass coated with Ag_2Se nanostructures with different numbers of coating cycles: (a) 5, (b) 9; Water CA measurements of glass coated with Ag_2Se nanostructures with different numbers of coating cycles and then treated by an ethanol solution of *n*-dodecanethiol: (c) 1, (d) 3, (e) 5, (f) 5, (g) 9, and (h) 11 coating cycles; Water CA measurements of glass coated with Ag_2Se nanostructures with different numbers of coating cycles and then treated by a methanol solution of 2% (*v*/*v*) 1H,1H,2H,2H-perfluorodecyltriethoxysilane: (i) 1, (j) 3, (k) 5, (l) 7, and (m) 9 coating cycles

Figure 6 and Movie S-1 in the ESM show a water droplet on a glass plate (coated 5 times with the as-synthesized Ag_2Se nanobowls, followed by a methanol solution of *n*-dodecanethiol) with a sliding angle of 1°.

This work confirms that the surface wettability of solid can be tuned via combining the formation of physical roughness with chemical surface treatment.

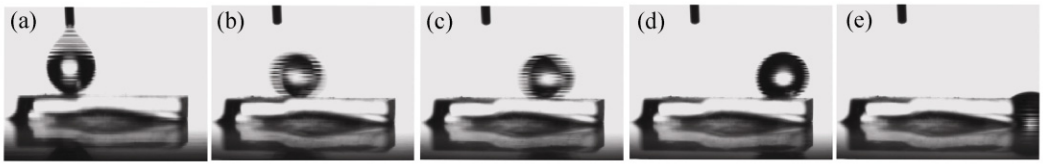

Figure 6 Sliding angle measurements with glass coated 5 times with Ag_2Se nanoplates and then treated by an ethanol solution of *n*-dodecanethiol

3. Conclusions

We have succeeded in developing a facile solvothermal method for the preparation of semiconductor plate-like β-Ag_2Se nanostructures showing both superhydrophobicity and photocatalytic properties. The as-obtained β-Ag_2Se nanostructures exhibited excellent photocatalytic activity for the degradation of RhB under UV light irradiation: the degradation of RhB reached as high as 89.8% after 15 h, which can be attributed to the special morphology and high specific surface area of the material. Additionally, the β-Ag_2Se nanostructures display superhydrophobic characteristics, with the water CA value being over 150°, with a sliding angle of 1°. This is a result of the surface being composed of micro- and nanostructures, similar to a lotus leaf, which strongly repel water. This approach provides a new strategy to generate novel multifunctional semiconductor Ag_2Se nanostructures with potential industrial applications, including photodegradation and self-cleaning for protection of Ag_2Se devices.

4. Experimental

4.1 Synthesis

$AgNO_3$ (analytical reagent, AR), selenophene (C_4H_4Se, AR), and aniline ($C_6H_5NH_2$, AR) were purchased and used without further purification. In a typical synthesis, 4 mmol of $AgNO_3$ was added to 20 mL of $C_6H_5NH_2$ with stirring for 1 h to form solution A. 0.5 mmol of C_4H_4Se was dissolved in 20 mL of $C_6H_5NH_2$ with stirring for 30 min and to form solution B. Solution B was added to solution A with stirring for 30 min at room temperature. Then, the mixture was sealed in a 50 mL Teflon-lined autoclave, heated to 240 °C, and maintained at this temperature for 10 h. After the autoclave was cooled down to room temperature naturally, the products were collected and washed by centrifugation at 5000 r/min for 5 min using deionized water and then absolute alcohol. The washing-cycle was repeated twice. Then, the products were treated with 4 mol/L HNO_3 for 0.5 h followed by washing three times using deionized water, and then treated by 20 mol/L NaOH for 1 h, and washed four times with deionized water. Finally, the products were washed using absolute alcohol, followed by drying at 60 °C for 6 h.

4.2 Characterization

XRD patterns were obtained using an X-ray diffractometer (Bruker D8 Advance) with Cu Kα radiation (λ = 1.5418 Å, operating at 40 kV and 40 mA) in the 2θ range from 10° to 70°. Raman spectra were recorded on a Renishaw RM-1000 laser Raman microscope with excitation from the 514.5 nm line of an Ar-ion laser with a power of about 5 mW. FE-SEM images were obtained using a JEOL JSM-7401F instrument. HRTEM images were recorded on a JEOL JEM-2010 electron microscope, operating at 200 kV. PL spectra were obtained using a fluorescence spectrophotometer (PerkinElmer LS55).

4.3 Photocatalytic activity tests

A 250 W high-pressure mercury lamp (Beijing Huiyixin Electric-light Source Technology Development Co.) was positioned inside a cylindrical vessel and surrounded by a circulating water jacket to cool the lamp. 30 mg of Ag_2Se catalyst was suspended in 30 mL of an aqueous solution of 10^{-5} mol/L RhB. The solution was continuously stirred for about 30 min at room temperature to ensure the establishment of an

adsorption–desorption equilibrium between the photocatalyst, RhB, and water before irradiation. The distance between the light source and the bottom of the solution was about 10 cm. The concentration of RhB was monitored using a UV–vis spectrometer (Unico Corp. UV-2102PC). The pH values of RhB solutions were adjusted by adding HCl or NaOH solution.

4.4 Wetting behavior tests

Water CA and sliding angle measurements were carried out with a water droplet (drop volume 8 μL or 8.5 μL) by using an optical contact angle meter (DataPhysics Inc., OCA 20) at room temperature.

Acknowledgements

The authors gratefully acknowledge the financial support from the National Natural Science Foundation of China (Nos. 20921001 and 20535020), the Innovation Method Fund of China (No. 20081885189), and the National High Technology Research and Development Program of China (No. 2009AA03Z321).

Electronic Supplementary Material: Supplementary material (SEM images of different samples, temporal UV–vis absorption spectral changes observed for the RhB solutions in the presence of different Ag_2Se photocatalysts, XRD pattern of the Ag_2Se nanoplates after photocatalytic reaction and a movie of the sliding angle measurement for glass modified by the as-synthesized complex Ag_2Se nanostructures followed by *n*-dodecanethiol solution) is available in the online version of this article at http://dx.doi.org/10.1007/s12274-010-0057-x and is accessible free of charge.

References

[1] van Blaaderen, A. Materials scienceColloids get complex. *Nature* **2006**, *439*, 545–546.

[2] Zhu, J.; Peng, H.; Marhall, A. F.; Barnett, D. M.; Nix, W. D.; Cui, Y. Formation of chiral branched nanowires by the Eshelby Twist. *Nat. Nanotechnol.* **2008**, *3*, 477–481.

[3] Krishna, K. S.; Mansoori, U.; Selvi, N. R.; Eswaramoorthy, M. Form emerges from formless entities: Temperature-induced self-assembly and growth of ZnO nanoparticles into zeptoliter bowls and troughs. *Angew. Chem. Int. Ed.* **2007**, *46*, 5962–5965.

[4] Hornyak, G. L.; Dutta, J.; Tibbals, H. F.; Rao, A. K. *Introduction to Nanoscience*; CRC Press: Boca Raton, USA, 2008.

[5] Schoen, D. T.; Xie, C.; Cui, Y. Electrical switching and phase transformation in silver selenide nanowires. *J. Am. Chem. Soc.* **2007**, *129*, 4116–4117.

[6] Cui, Y.; Chen, G.; Ren, J.; Shao, M.; Xie, Y.; Qian, Y. Solvothermal syntheses of β-Ag_2Se crystals with novel morphologies. *J. Solid State Chem.* **2003**, *172*, 17–21.

[7] Kobayashi, M. Review on structure and dynamic properties of silver chalcogenides. *Solid State Ionics*. **1990**, *39*, 121–149.

[8] Wang, H.; Qi, L. Controlled synthesis of Ag_2S, Ag_2Se, and Ag nanofibers using a general sacrificial template and their application in electronic device fabrication. *Adv. Funct. Mater.* **2008**, *18*, 1249–1256.

[9] Gates, B.; Mayers, B.; Wu, Y.; Sun, Y.; Cattle, B.; Yang, P.; Xia, Y. Synthesis and characterization of crystalline Ag_2Se nanowires through a template-engaged reaction at room temperature. *Adv. Funct. Mater.* **2002**, *12*, 679–686.

[10] Ma, D.; Zhang, M.; Xi, G.; Zhang, J.; Qian, Y. Fabrication and characterization of ultralong Ag/C nanocables, carbonaceous nanotubes, and chainlike β-Ag_2Se nanorods inside carbonaceous nanotubes. *Inorg. Chem.* **2006**, *45*, 4845–4849.

[11] Erbil, H. Y. *Surface Chemistry of Solid and Liquid Interfaces*; Blackwell Publishing: Oxford, UK, 2006.

[12] Xia, Y. Nanomaterials at work in biomedical research. *Nat. Mater.* **2008**, *7*, 758–760.

[13] Lahann, J. Environmental nanotechnology—Nanomaterials clean up. *Nat. Nanotechnol.* **2008**, *3*, 320–321.

[14] Yuan, J.; Liu, X.; Akbulut, O.; Hu, J.; Suib, S. L.; Kong, J.; Stellacci, F. Superwetting nanowire membranes for selective absorption. *Nat. Nanotechnol.* **2008**, *3*, 332–336.

[15] Wu, J.; Yi, T.; Shu, T.; Yu, M.; Zhou, Z.; Xu, M.; Zhou, Y.; Zhang, H.; Han, J.; Li, F.; Huang, C. A core-modified rubyrin with meso-aryl substituents and phenanthrene-fused pyrrole rings: A highly conjugated near-infrared dye and Hg^{2+} probe. *Angew. Chem. Int. Ed.* **2008**, *47*, 1063–1067.

[16] Dorrer, C.; Rühe, J. Wetting of silicon nanograss: From superhydrophilic to superhydrophobic surfaces. *Adv. Mater.* **2008**, *20*, 159–163.

[17] Ma, M.; Gupta, M.; Li, Z.; Zhai, L.; Gleason, K. K.; Cohen, R. E.; Rubner, M. F.; Rutledge, G. C. Decorated electrospun fibers exhibiting superhydrophobicity. *Adv. Mater.* **2007**, *19*, 255–259.

[18] Zhu, Y.; Hu, D.; Wan, M.; Jiang, L.; Wei, Y. Conducting and superhydrophobic rambutan-like hollow spheres of polyaniline. *Adv. Mater.* **2007**, *19*, 2092–2096.

[19] Xia, F.; Ge, H.; Hou, Y.; Sun, T.; Chen, L.; Zhang, G.; Jiang, L. Multiresponsive surfaces change between superhydrophilicity and superhydrophobicity. *Adv. Mater.* **2007**, *19*, 2520–2524.

[20] Kozicki, M. N.; Mitkova, M.; Zhu, J.; Park, M. Nanoscale phase separation in Ag–Ge–Se glasses. *Microelectron. Eng.* **2002**, *63*, 155–159.

[21] Ogusu, K.; Kumagai, T.; Fujimori, Y. Thermal analysis and Raman scattering study on crystallization and structure of $Ag_x(As_{0.4}Se_{0.6})_{100-x}$ glasses. *J. Non-Cryst. Solids* **2003**, *324*, 118–126.

[22] Ge, J. -P.; Xu, S.; Liu, L. -P.; Li, Y. -D. A positive-microemulsion method for preparing nearly uniform Ag_2Se nanoparticles at low temperature. *Chem. Eur. J.* **2006**, *12*, 3672–3677.

[23] Yuan, J.; Li, W. -N.; Gomez, S.; Suib, S. L. Shape-controlled synthesis of manganese oxide octahedral molecular sieve three-dimensional nanostructures. *J. Am. Chem. Soc*. **2005**, *127*, 14184–14185.

[24] Sun, S.; Yang, D.; Villers, D.; Zhang, G.; Sacher, E.; Dodelet, J. P. Template- and surfactant-free room temperature synthesis of self-assembled 3D Pt nanoflowers from single-crystal nanowires. *Adv. Mater*. **2008**, *20*, 571–574.

[25] Jiao, C. M.; Wang, Z. Z.; Ye, Z.; Hu, Y.; Fan, W. C. Flame retardation of ethylene-vinyl acetate copolymer using nano magnesium hydroxide and nano hydrotalcite. *J. Fire Sci.* **2006**, *24*, 47–64.

[26] Zhang, S.; Fang, C.; Wei, W.; Jin, B.; Tian, Y.; Shen, Y.; Yang, J.; Gao, H. Synthesis and electrochemical behavior of crystalline Ag_2Se nanotubes. *J. Phys. Chem. C* **2007**, *111*, 4168–4174.

[27] Cao, H.; Qiu, X.; Luo, B.; Liang, Y.; Zhang, Y.; Tan, R.; Zhao, M.; Zhu, Q. Synthesis and room-temperature ultraviolet photoluminesence properties of zirconia nanowires. *Adv. Funct. Mater*. **2004**, *14*, 243–246.

[28] Li, X.; Kikugawa, N.; Ye, J. A comparison study of rhodamine B photodegradation over nitrogen-doped lamellar niobic acid and titanic acid under visible-light irradiation. *Chem. Eur. J*. **2009**, *15*, 3538–3545.

[29] Kawahara, T.; Konishi, Y.; Tada, H.; Tohge, N.; Nishii, J.; Ito, S. A patterned TiO_2(anatase)/TiO_2(rutile) bilayer-type photocatalyst: Effect of the anatase/rutile junction on the photocatalytic activity. *Angew. Chem. Int. Ed.* **2002**, *41*, 2811–2813.

[30] Wu, J. M.; Zhang, T. W. Photodegradation of rhodamine B in water assisted by titania films prepared through a novel procedure. *J. Photochem. Photobiol. A* **2004**, *162*, 171–177.

[31] Ferhat, M.; Nagao, J. Thermoelectric and transport properties of β-Ag_2Se compounds. *J. Appl. Phys.* **2000**, *88*, 813–816.

[32] Kumar, M. C. S.; Pradeep, B. Transport properties of silver selenide thin films from 100 to 300 K. *Bull. Mater. Sci.* **2002**, *25*, 407–411.

[33] Liu, Z. L.; Guo, B.; Hong, L.; Jiang, H. X. Physicochemical and photocatalytic characterizations of TiO_2/Pt nanocomposites. *J. Photochem. Photobiol. A.* **2005**, *174*, 81–88.

[34] Hidaka, H.; Zhao, J.; Pelizzetti, E.; Serpone, N. Photo-degradation of surfactants. 8. Comparison of photocatalytic processes between anionic sodium dodecylbenzenesulfonate and cationic benzyldodecyldimethylammonium chloride on the TiO_2 surface. *J. Phys. Chem*. **1992**, *96*, 2226–2230.

[35] Chen, C.; Zhao, W.; Lei, P.; Zhao, J.; Serpone, N. Photosensitized degradation of dyes in polyoxometalate solutions versus TiO_2 dispersions under visible-light irradiation: Mechanistic implications. *Chem. Eur. J.* **2004**, *10*, 1956–1965.

[36] Zhang, L.; Wang, W.; Zhou, L.; Xu, H. Bi_2WO_6 nano- and microstructures: Shape control and associated visible-light-driven photocatalytic activities. *Small* **2007**, *3*, 1618–1625.

[37] Fu, H.; Pan, C.; Yao, W. Zhu, Y. Visible-light-induced degradation of rhodamine B by nanosized Bi_2WO_4. *J. Phys. Chem. B.* **2005**, *109*, 22432–22439.

[38] Xu, H.; Zhang, L. Z. Controllable one-pot synthesis and enhanced photocatalytic activity of mixed-phase TiO_2 nanocrystals with tunable brookite/rutile ratios. *J. Phys. Chem. C* **2009**, *113*, 1785–1790.

[39] Zheng, H.; Liu, K. Y.; Cao, H. Q.; Zhang, X. R. *L*-lysine-assisted synthesis of ZrO_2 nanocrystals and their application in photocatalysis. *J. Phys. Chem. C* **2009**, *113*, 18259–18263.

[40] Chen, L. Y.; Liang, Y.; Zhang, Z. D. Corundum-type In_2O_3 urchin-like nanostructures: Synthesis derived from orthorhombic InOOH and application in photocatalysis. *Eur. Inorg. Chem.* **2009**, *7*, 903–909.

[41] Wang, C. H.; Song, Y. Y.; Zhao, H. W.; Xia, X. H. Semiconductor supported biomimetic superhydrophobic gold surfaces by the galvanic exchange reaction. *Surf. Sci.* **2006**, *600*, L38–L42.

[42] Zhao, Y.; Lu, Q.; Chen, D.; Wei, Y. Superhydrophobic modification of polyimide films based on gold-coated porous silver nanostructures and self-assembled monolayers. *J. Mater. Chem.* **2006**, *16*, 4504–4509.

[43] Li, Y.; Huang, X. J.; Heo, S. H.; Li, C. C.; Choi, Y. K.; Cai, W. P.; Cho, S. O. Superhydrophobic bionic surfaces with

hierarchical microsphere/SWCNT composite arrays. *Langmuir* **2007**, *23,* 2169–2174.

[44] Li, Y.; Li, C. C.; Cho, S. O.; Duan, G. T.; Cai, W. P. Silver hierarchical bowl-like array: Synthesis, superhydrophobicity, and optical properties. *Langmuir* **2007**, *23*, 9802–9807.

[45] Kong, L.; Chen, X.; Yang, G.; Yu, L.; Zhang, P. Preparation and characterization of slice-like $Cu_2(OH)_3NO_3$ superhydrophobic structure on copper foil. *Appl. Surf. Sci.* **2008**, *254*, 7255–7258.

[46] Chen, X.; Kong, L.; Dong, D.; Yang, G.; Yu, L.; Chen, J.; Zhang, P. Synthesis and characterization of superhydrophobic functionalized $Cu(OH)_2$ nanotube arrays on copper foil. *Appl. Surf. Sci.* **2009**, *255*, 4015–4019.

[47] de Givenchy, E. P. T.; Amigoni, S.; Martin, C.; Andrada, G.; Caillier, L.; Géribaldi, S.; Guittard, F. Fabrication of superhydrophobic PDMS surfaces by combining acidic treatment and perfluorinated monolayers. *Langmuir* **2009**, *25,* 6448–6453.

[48] Chen, X.; Kong, L.; Dong, D.; Yang, G.; Yu, L.; Chen, J.; Zhang, P. Fabrication of functionalized copper compound hierarchical structure with bionic superhydrophobic properties. *J. Phys. Chem. C* **2009**, *113,* 5396–5401.

[49] Wu, S.; Cao, H.; Yin, S.; Zhang, X.; Chernow, V. Biomineralization and superhydrophobicity of $BaCO_3$ complex nanostructures. *Inorg. Chem.* **2009**, *48*, 10326–10329.

[50] Cao, H.; Zheng, H.; Liu, K.; Fu, R. Single-crystalline semiconductor $In(OH)_3$ nanocubes with bifunctions: Superhydrophobicity and photocatalytic activity. *Cryst. Growth Des.* **2010**, *10*, 597–601.

[51] Song, H. -J.; Shen, X. -Q. Fabrication of functionalized aluminum compound petallike structure with superhydrophobic surface. *Surf. Interface Anal.* **2010**, *42*, 165–168.